

# MicroRNA Profiling in Paired Left and Right Eyes, Lungs, and Testes of Normal Mice

Jiangcheng Shi,<sup>1,2</sup> Chengqing Hu,<sup>1,2</sup> Yuan Zhou,<sup>1</sup> Chunmei Cui,<sup>1</sup> Jichun Yang,<sup>1</sup> and Qinghua Cui<sup>1</sup>

<sup>1</sup>Department of Biomedical Informatics, Department of Physiology and Pathophysiology, Center for Noncoding RNA Medicine, MOE Key Lab of Cardiovascular Sciences, School of Basic Medical Sciences, Peking University, 38 Xueyuan Rd., Beijing 100191, China

**Physiological and pathophysiological differences widely exist in paired organ systems. However, the molecular basis for these differences remains largely unknown. We previously reported that there exist differentially expressed miRNAs (DEMs) in the left and right kidneys of normal mice. Here, we identified the DEMs in the left and right eyes, lungs, and testes of normal mice via RNA sequencing. As a result, we identified 26 DEMs in eyes, with 23 higher and 3 lower in the left eyes compared with right eyes; 21 DEMs in lungs, with 15 higher and 6 lower in the left lungs compared with right lungs; and 54 DEMs in testes, with 6 higher and 48 lower in the left testes compared with right testes. Ten microRNAs (miRNAs) were further examined by quantitative PCR assays, and seven of these were confirmed. In addition, correlation analysis was performed between paired organ miRNA expressions and diverse body fluid miRNA expressions. Finally, we explored the functions and networks of DEMs and performed biological process and pathway enrichment analysis of target genes for DEMs, providing insights into the physiological and pathophysiological differences between the two entities of paired organs.**

## INTRODUCTION

Diseases of the paired organ systems in the human body—including the eyes, lungs, and testes—form a large proportion of all diseases. For example, retinoblastoma is the most common intraocular tumor in children; approximately 1 in 20,000 children are affected by retinoblastoma worldwide.<sup>1</sup> Furthermore, various lung diseases have become the leading cause of human deaths; among them, lung cancer is the leading cause of cancer-related deaths worldwide.<sup>2</sup> Pneumonia caused by the coronavirus disease 2019 (COVID-19), of which there was a recent breakout in Wuhan, China, is rapidly spreading throughout many countries.<sup>3</sup> Moreover, of reproductive system diseases, testicular cancer is the most common cancer diagnosed in males under the age of 40 years.<sup>4</sup>

To be particular, the left and right organs in most paired organ systems are asymmetric, and it has been previously reported that not only the anatomical structure but also the morbidity of some paired organs is different between the left and right sides. Munuera-Gifre et al.<sup>5</sup> have demonstrated that retinal lesions are not distributed randomly but rather follow a determined pattern. They found that the left eye exhibits more microaneurysms/hem-

orrhages and hard exudates of a greater density in the central retina than the right eye. Similarly, on evaluating the pathological anatomy of patients with COVID-19-related pneumonia, X-ray images showed rapid progression of pneumonia and some differences between the left and right lungs.<sup>6</sup> In a study performed by Vaganée et al.,<sup>7</sup> approximately 78%–93% of varicoceles are shown to appear on the left side, and a smaller left testis is more frequently observed on comparing patients with varicoceles and healthy adolescents. Collectively, there are differences in pathophysiological and biological functions between the left and right sides of paired organs, but the underlying molecular basis causing these differences remains unknown.

MicroRNAs (miRNAs) are an important class of noncoding RNAs, which are widely involved in the post-transcriptional regulation of gene expression and play important roles in physiological processes as well as the development of various diseases. Recently, miRNAs have been found to be widely involved in the development of many diseases associated with the eyes, lungs, and testes. For example, it was reported that rno-miR-138-5p regulates early diabetic retinopathy by promoting cell proliferation via targeting *Nova1* (NOVA alternative splicing regulator 1) in rat.<sup>8</sup> Besides, hsa-miR-4651 inhibits the progression of non-small-cell lung cancer by targeting *BRD4* (bromodomain-containing protein 4).<sup>9</sup> Moreover, hsa-miR-371a-3p can be used as an informative biomarker for follow-up in patients with testicular germ cell cancer.<sup>10</sup>

We have previously revealed that differentially expressed miRNAs (DEMs) exist between the left and right kidneys of normal mice,<sup>11</sup> providing new insights into the physiological and pathophysiological

Received 6 April 2020; accepted 6 July 2020;  
<https://doi.org/10.1016/j.omtn.2020.07.006>.

<sup>2</sup>These authors contributed equally to this work.

**Correspondence:** Jichun Yang, Department of Biomedical Informatics, Department of Physiology and Pathophysiology, Center for Noncoding RNA Medicine, MOE Key Lab of Cardiovascular Sciences, School of Basic Medical Sciences, Peking University, 38 Xueyuan Rd., Beijing 100191, China.  
**E-mail:** yangj@bjmu.edu.cn

**Correspondence:** Qinghua Cui, Department of Biomedical Informatics, Department of Physiology and Pathophysiology, Center for Noncoding RNA Medicine, MOE Key Lab of Cardiovascular Sciences, School of Basic Medical Sciences, Peking University, 38 Xueyuan Rd., Beijing 100191, China.  
**E-mail:** cuiqinghua@bjmu.edu.cn



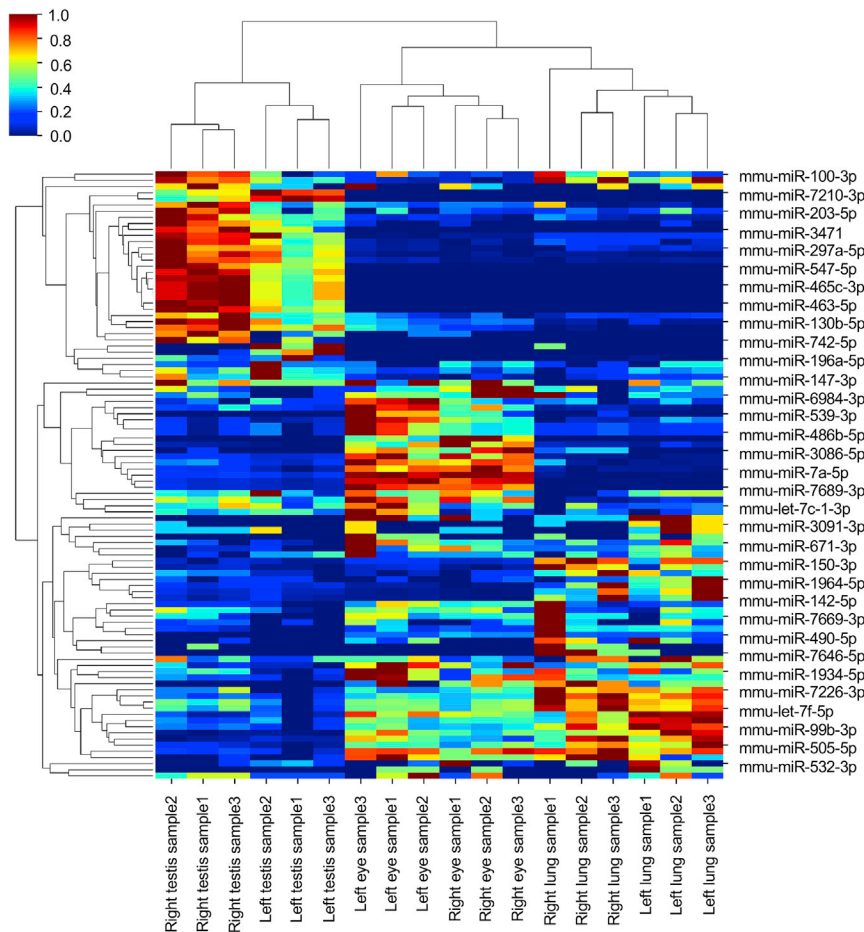


**Figure 1. Heatmap of DEMs**

Significantly DEMs between the left and right eyes, lungs, and testes.

The DEMs are shown in [Tables S1, S2, and S3](#). Heatmap and dendrogram cluster analyses demonstrated that we can well distinguish the left samples from the right ones with the help of these DEMs ([Figure 1A](#)).

We further investigated some biological features of these DEMs. We found that DEMs are distributed on both autosomes and the X chromosome ([Figure S1A](#)). Interestingly, the DEMs in the testes were found to make up a sizeable proportion of the X chromosome (24%; 13/54). No significant differentially expressed distribution was observed. Next, the allocation of DEMs in the three organs between autosomes and sex chromosomes was shown in [Figure S1B](#). Finally, evolutionary conservation is also an important feature to explore the function of miRNAs. To illustrate the evolutionary conservation of these DEMs, we first divided miRNAs into three groups as described previously,<sup>12</sup> using the miRNA family resources provided by miRbase (v.21);<sup>13</sup> namely, a mammal-specific group, a vertebrate-specific group and a group for miRNAs represented in other more distal species such as invertebrate animals. No significant difference in conservation was observed

differences between the two sides of kidneys and facilitating the diagnosis and treatment of lateralized kidney diseases. Thus far, it is unclear whether the miRNA expression profiles are different between two sides of the eyes, lungs, and testes. Accordingly, in this study, we first identified DEMs in these paired organs of normal mice using RNA sequencing (RNA-seq) technology and then performed bioinformatic analyses on these miRNAs.

## RESULTS

### miRNA Expression Profiles in Paired Organ Systems of a Normal C57BL/6J Mouse

To determine the potential DEMs concerning physiological processes in paired organ systems, the miRNA profiles in the eyes, lungs, and testes of mice were determined using RNA-seq technology at BGI Genomics (Beijing, China). As a result, a total of 1,431 miRNA signals were detected in the paired eyes, lungs, and testes. We identified 26 DEMs in the eyes (with the expression of 23 miRNAs being higher and 3 being lower in the left eyes than in the right ones), 21 DEMs in the lungs (with the expression of 15 miRNAs being higher and 6 being lower in the left lungs than in the right ones), and 54 DEMs in the testes (with the expression of 6 miRNAs being higher and 48 being lower in the left testes than in the right ones).

between DEMs and non-DEMs. The distribution of miRNAs in the three organs among the three different groups is shown in [Figure S1C](#).

### Validation of DEMs

To further validate the accuracy of RNA-seq, we randomly selected 10 miRNAs homologous with human miRNAs for verification. Bulge-loop real-time PCR analysis of the 10 selected miRNAs showed that the expression levels of seven of these miRNAs are different between the left and right organs in paired eyes, lungs, and testes of mice, and this result was consistent with the results of RNA-seq. We found that mmu-miR-142a-5p and mmu-miR-187-5p have significantly higher expression levels, whereas mmu-miR-203b-3p has a lower expression level in the left eyes than in the right eyes ([Figures 2A–2C](#)). Further, we found that the expression levels of mmu-miR-107-5p and mmu-miR-122b-5p are significantly higher, whereas that of mmu-miR-100-3p is lower in the left lungs than in the right lungs ([Figures 2D–2F](#)). Moreover, the expression level of mmu-miR-204-5p was confirmed to be lower in left testes than in right ones ([Figure 2H](#)). Finally, the real-time PCR results of the remaining three miRNAs were not consistent with the RNA-seq results. The trend observed with regard to the expression level of mmu-miR-148a-5p in the left and right lungs after PCR analysis was in contrast to that observed

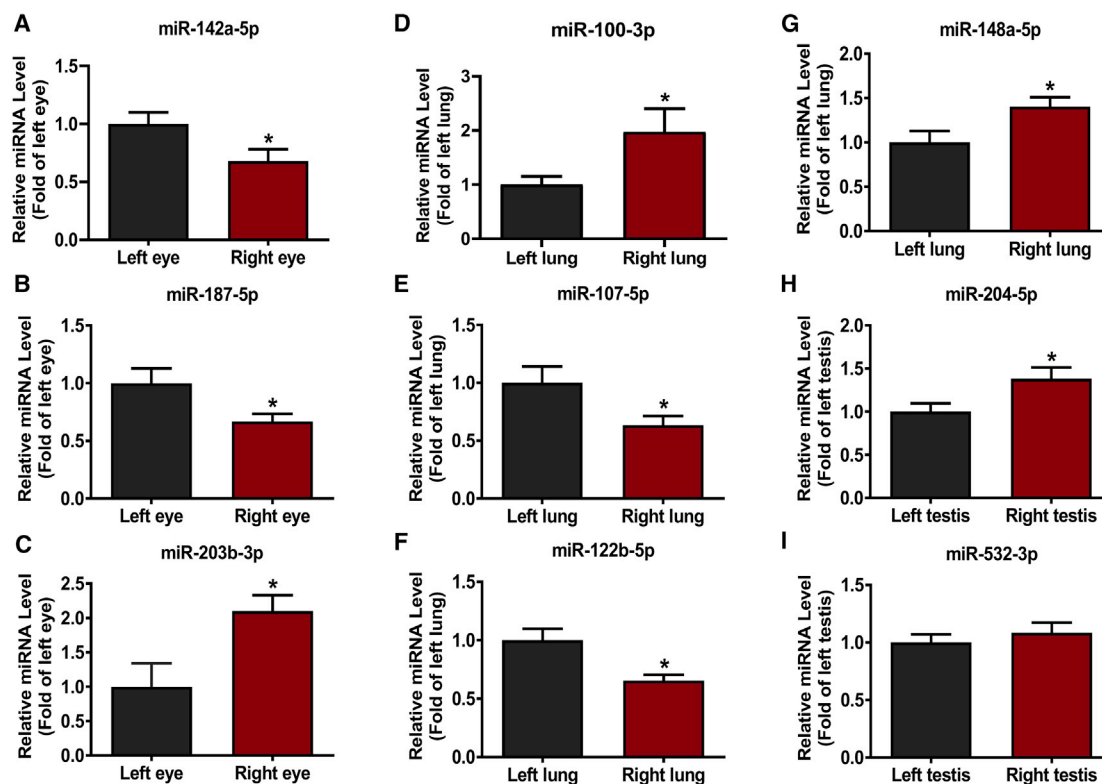


**Figure 2. Validation of DEMs in the Paired Organ Systems of C57BL/6J Mice**

(A–C) The expression levels of mmu-miR-142a-5p (A), mmu-miR-187-5p (B), and mmu-miR-203b-5p (C) in the eyes. (D–G) The expression levels of mmu-miR-100-3p (D), mmu-miR-107-5p (E), mmu-miR-122b-5p (F), and mmu-miR-148a-5p (G) in the lungs. (H and I) The expression levels of mmu-miR-204-5p (H) and mmu-miR-532-3p (I) in the testes. The data were normalized to the left organ (ns = 10–15; mean  $\pm$  SEM). \* $p < 5e-2$ , versus left organ.

with RNA-seq (Figure 2G). Further, we observed no significant difference in the expression level of mmu-miR-532-3p in paired testes (Figure 2I). In addition, the expression level of mmu-miR-297a-5p in the eyes was not detected successfully, which may have resulted because of the degradation of some RNA during the procedure. Overall, the real-time PCR data supported the accuracy of RNA-seq data.

#### Comparison of miRNA Expression Profiles in Paired Organs with Those in Various Body Fluids

In the past decade, circulating miRNAs have been proposed to be useful in diagnostics and prognosis as biomarkers for diseases,<sup>14</sup> and their expression profiles have been correlated with those of miRNAs in tissues. Here, we compared the association of miRNA expression profiles in the left and right organs of mice with those in mouse body fluids, homologous miRNA expression profiles in rat arterial plasma and venous plasma, and homologous miRNA expression profiles in diverse human body fluids. As a result, we found that the expression profiles in the left and right organs of mice are highly correlated with those in the plasma, bile, and urine of mice ( $\rho > 0.60$ ,  $p < 1e-50$  in plasma;  $\rho > 0.50$ ,  $p < 1e-20$  in bile; and  $\rho > 0.3$ ,  $p < 1e-4$  in urine; Figures 3A–3C). Particularly, the miRNA expression profiles in the left and right lungs showed higher correlations with the expression profiles in the three body fluids of mice, but

the paired testes showed lower correlations; this finding was consistent with the previous findings in humans.<sup>15</sup> Interestingly, we found a significant difference in correlation coefficients between miRNA expression profiles in left and right lungs and those in rat arterial plasma ( $p = 3.6e-2$ , matched-pair t test, Figure 3D), but there was no difference between miRNA expression profiles in left and right lungs and those in rat venous plasma (Figure 3E). On evaluating the correlations between miRNA expression profiles in the left and right organs of mice and homologous miRNA expression profiles in diverse human body fluids, the patterns of correlations observed between paired organs in mice and diverse human body fluids were similar to those observed between paired organs and body fluids in mice (Figures 3F–3I). Collectively, we demonstrated that the expression profiles of miRNA in the left and right organs in mice are significantly correlated with those in various body fluids (Table S4).

#### Functional Enrichment Analysis of the DEMs

Using the TAM v.2.0 tool, we found that the homologous human miRNAs with higher expression levels in the left eyes, left lungs, and right testes are significantly enriched in 9, 26, and 28 functional terms, respectively. The miRNAs with higher expression levels in the left eyes were mainly involved in the following functions: skeletal muscle cell differentiation, inflammation, response to hypoxia,

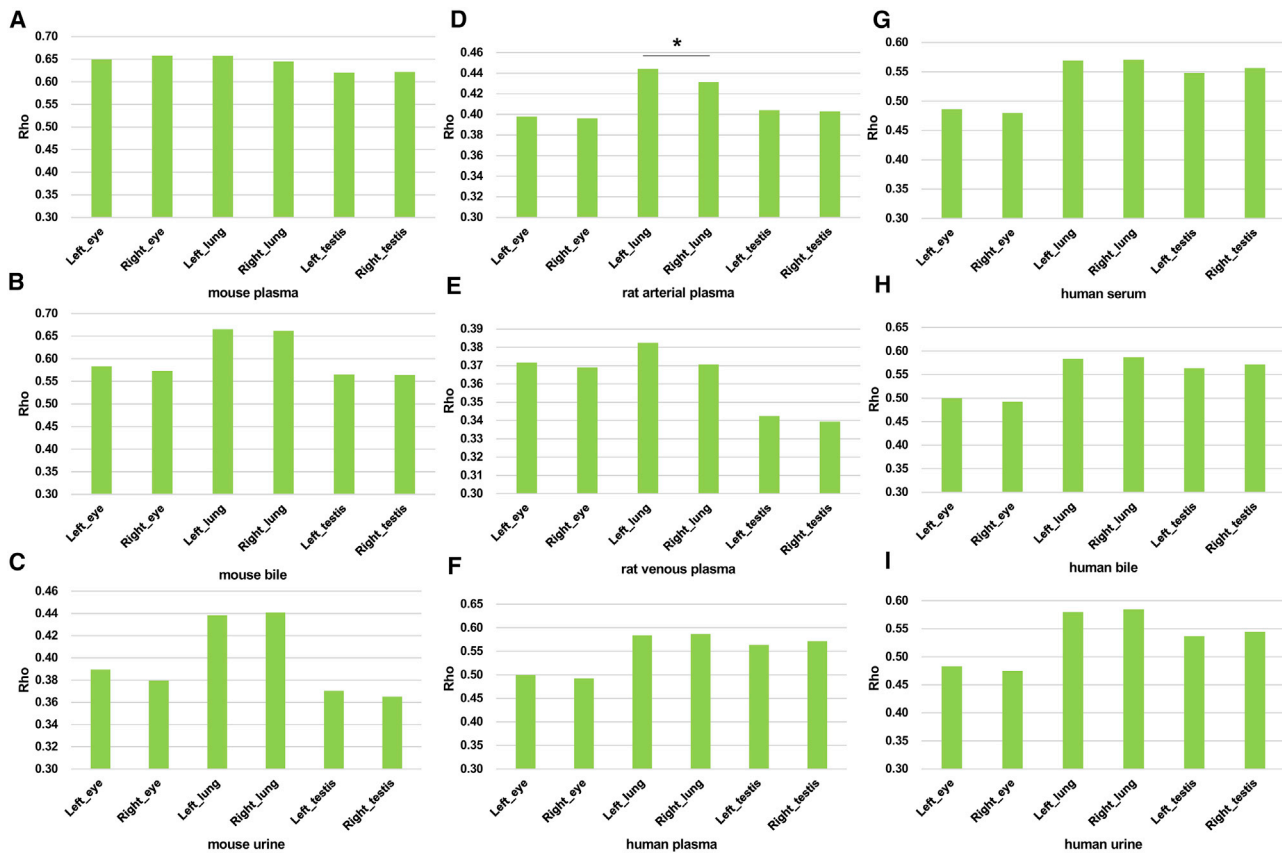


**Figure 3. Comparison of miRNA Expression Profiles in Paired Organs with miRNA Expression Profiles in Various Body Fluids**

(A–I) Expression correlation between paired organ miRNAs and miRNAs in plasma (A), bile (B), and urine (C) of mice; homologous miRNAs in arterial plasma (D) and venous plasma (E) of rats; and homologous miRNAs in plasma (F), serum (G), bile (H), and urine (I) of humans. Asterisk indicates significant difference in correlation coefficients between miRNA expression profiles in the left and right lungs and miRNA expression profile in arterial plasma of rats ( $p < 5e-2$ ), according to matched-pair *t* test.

T cell differentiation, smooth muscle cell proliferation, cytokine secretion, hematopoiesis, apoptosis, tumor suppressor miRNAs (Figure 4A). This suggested that the DEMs in the left eyes may contribute to the development of eye muscles and defense against disease. Besides, the highly expressed miRNAs in the left lungs were mainly enriched in functional terms such as adipogenesis, inflammation, lipid metabolism, insulin resistance, regulation of stem cell, circadian rhythm (Figure 4B). Moreover, the top five functional terms associated with highly expressed miRNAs in the right testes were neural stem cell differentiation, cell death, tumor suppressor miRNAs, aging, and adipocyte differentiation (Figure 4C). Notably, the functional terms associated with disease defense such as inflammation, tumor suppressor miRNAs, T cell differentiation, and immune response were found to be enriched in all these organs. Surprisingly, we did not observe any significant functional terms for the miRNAs with higher expression levels in the right eyes, right lungs, and left testes.

#### Functional Similarity Network of the DEMs

We calculated the functional similarity of DEMs by implementing the MISIM algorithm, which is based on the miRNA disease associa-

tion dataset in the Human MicroRNA Disease Database (HMDD). Finally, we filtered miRNAs with a similarity higher than 0.2 and constructed a functional similarity network using Cytoscape software.

Among the network of DEMs in the eyes (Figure 5A), miR-150 and miR-187 have been extensively studied. Shi et al.<sup>16</sup> have reported that the deletion of mmu-miR-150 can significantly increase retinal pathological angiogenesis in high fat diet (HFD)-induced type 2 diabetic mice. In another study, the researchers revealed that rno-miR-187 up-regulation alleviates oxidative stress injury in retina tissues of rat with ocular hypertension,<sup>17</sup> which is closely associated with the development of retinal disease. Further, among the network of DEMs in the lungs (Figure 5B), miR-107, miR-125a, miR-148a, and miR-100 showed high similarity; and in literature research, we found that they play a role in many common lung diseases, such as lung cancer, small-cell lung cancer, and non-small-cell lung cancer. Among them, miR-125a is mostly associated with lung diseases (Table 1 shows the detailed associations of miR-125a with lung diseases). The results indicated that these miRNAs may have a synergistic effect in the occurrence and development of lung diseases. Finally, as shown in the network of

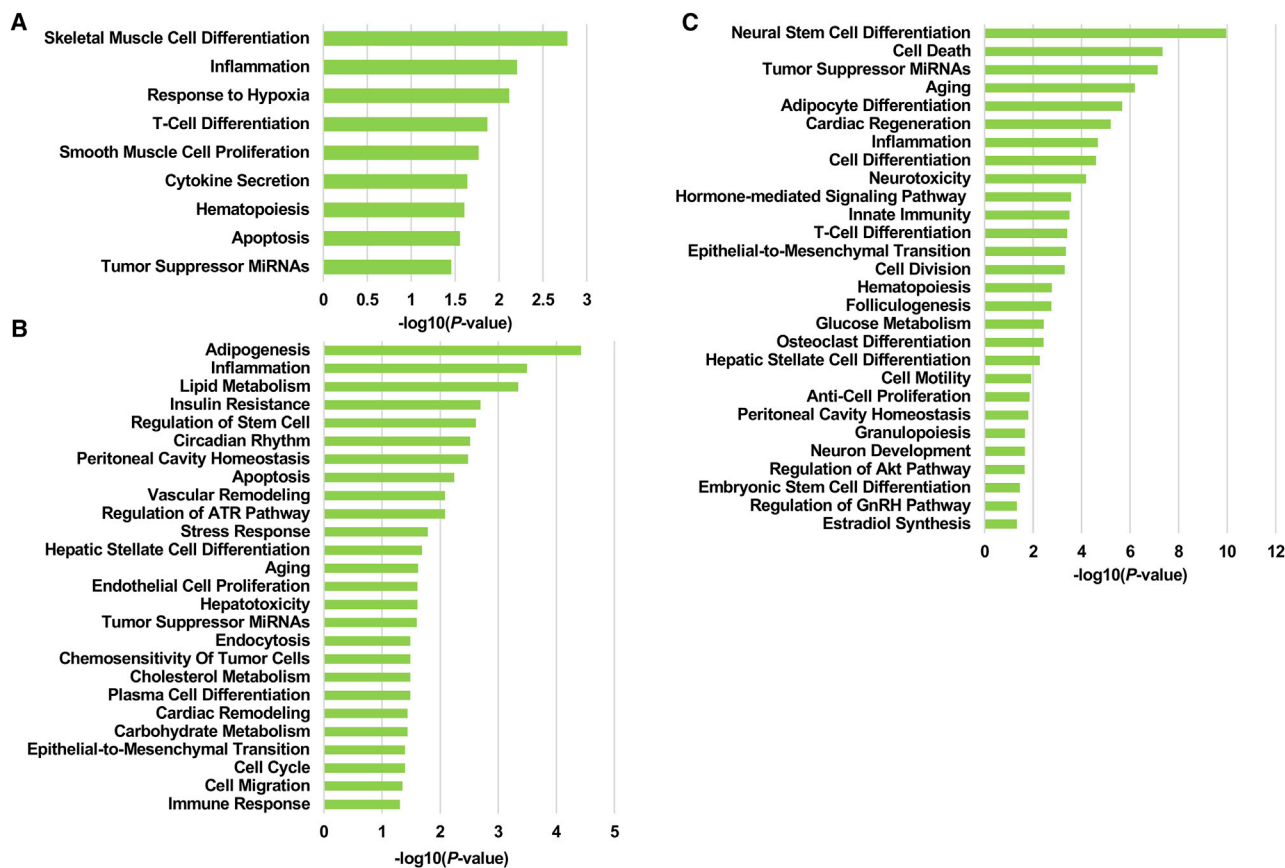


**Figure 4. Functional Enrichment Analysis of the DEMs**

(A–C) Enriched biological functions associated with the DEMs upregulated in the left eyes (A), left lungs (B), and right testes (C). The length of each bar is the value of  $-\log_{10}$  (p value).

DEMs in the testes (Figure 5C), many functionally similar miRNAs play important roles in the pathophysiological progress in the testes. In the study by Abhari et al.,<sup>18</sup> hsa-miR-100 and hsa-let-7b in oligospermic patients were found to be possibly associated with the susceptibility and progression of infertility. Similarly, miR-191 and miR-10b were also reported to be associated with spermatogenesis,<sup>19,20</sup> and mmu-miR-10b was reported to be highly expressed in mouse spermatogonial stem cells (SSCs) *in vitro* and in enhanced SSC proliferation.<sup>10</sup> Moreover, hsa-miR-302 was inferred to act as an oncogene in human testicular germ cell tumors by inducing the expression of *SPRY4* and activating the mitogen-activated protein kinase (MAPK)/ERK pathway while inhibiting apoptosis by increasing survivin expression.<sup>21</sup>

All these findings further our understanding of the miRNA functions in paired-organ-related diseases and provide a basis for the diagnosis, treatment, and prevention of these diseases.

#### Target Analysis for DEMs

Given that the main function of miRNA is to regulate the expression of target genes to participate in various physiological and patho-

physiological activities, we conducted a biological process and pathway enrichment analysis for the target genes of DEMs. The results showed that these target genes are significantly enriched in various biological processes. The target genes of DEMs in the left eyes were most enriched in cell adhesion (Figure 6A), which plays an important role in the pathogenesis of various eye diseases.<sup>22,23</sup> Similarly, the target genes of DEMs in the right eyes were enriched in the positive regulation of epithelial cell proliferation, DNA repair, and B cell activation, among other processes (Figure 6B). Interestingly, the target genes of DEMs in the left and right lungs were both enriched in tumor-related processes, such as regulation of tumor necrosis factor production, p53 signaling pathway, and DNA double-strand break repair (Figures 6C and 6D). Furthermore, the enrichment results in the right testes showed that the target genes were associated with urogenital system development, and the target genes in both sides were enriched in the physiological process of behavior regulation, including subentries such as learning and memory (Figures 6E and 6F). Taken together, the results of enrichment analysis indicated that the target genes regulated by these DEMs in paired organs have various functions in diverse physiological processes and pathways.

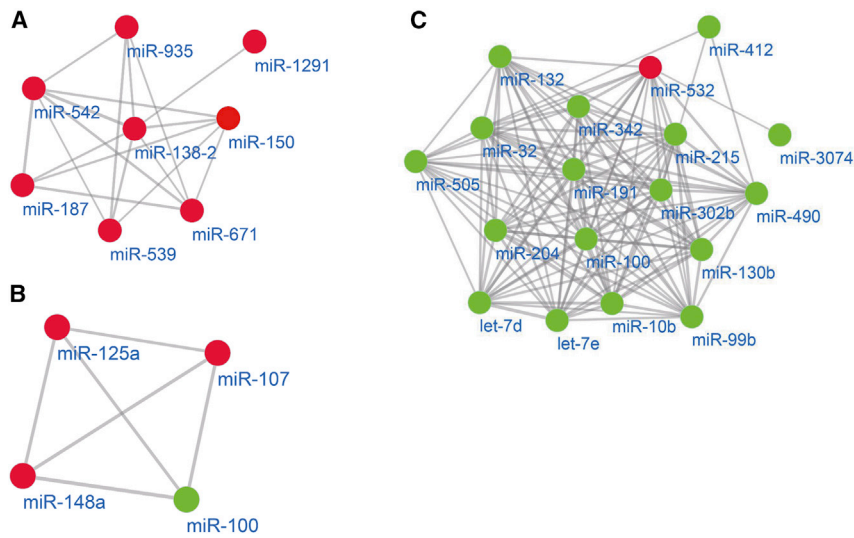


**Figure 5. Functional Similarity Network of the DEMs**

(A–C) Each red/green node represents an upregulated miRNA in the left/right eye (A), the left/right lung (B), and the left/right testis (C), respectively.

## DISCUSSION

Many organs in the human body exist in pairs; e.g., the eyes, lungs, kidneys and testes. The anatomical structures of these organs under different physiological and pathological conditions, as well as the incidence rates of pathologies in many pairs of organs, are different.

Anisometropia is a condition in which the refractive errors differ between the two eyes.<sup>24</sup> Although there is substantial evidence of the axial nature of anisometropia,<sup>25–27</sup> little is known about the biology basis. Further, pulmonary agenesis is an uncommon congenital anomaly resulting from the failure of pulmonary development beyond the carina, and unilateral lesions constitute 70% of cases.<sup>28</sup> However, the details of the reasons of the case are still unknown. In addition, varicoceles mostly present at the beginning of puberty and are observed in approximately 14%–20% of adolescents. It appears on the left side in 78%–93% of all cases.<sup>29,30</sup> Again, the molecular bases behind all these paired organ pathologies are unclear and need to be further elucidated.

miRNAs represent an important class of noncoding RNA molecules and accomplish a remarkable variety of biological functions.<sup>31,32</sup> Here, we identified DEMs in multiple paired organs such as the eyes, lungs, and testes using RNA-seq technology in normal C57BL/6J mice. Subsequently, seven out of 10 DEMs were validated by quantitative PCR assays, confirming the accuracy of RNA-seq analysis results. Moreover, we indicated intriguing expression correlations between paired organs and diverse body fluids. In addition, functional enrichment analysis and network biology analysis demonstrated that DEMs are clearly involved in the corresponding paired-organ-related diseases. Finally, we also conducted a biological process and pathway enrichment analysis for the target genes of the DEMs, suggesting that the DEMs play important roles in various physiological processes and pathways by regulating the target genes.

We have, for the first time, detected the miRNA profiles in the paired organ systems of normal mice. These findings can provide some new insights into understanding the physiological and functional differences between the left and right sides of paired organs, and they can also help promote the diagnosis and treatment of some related diseases.

## MATERIALS AND METHODS

### Experimental Mice

In this study, 8- to 12-week-old male C57BL/6J mice (weight, 22–25 g) were used. All animals were bred and housed locally at 24°C ± 2°C and were acclimated to standard laboratory conditions (12-h:12-h light:dark cycle) with free access to rodent feed and water. All animal care and experimental protocols complied with the Animal Management Rules of the Ministry of Health of the People's Republic of China and the Guide for the Care and Use of the Laboratory Animals of Peking University. All animal protocols were approved by the Animal Research Committee of the Peking University Health Science Center.

### RNA-Seq Analysis for the Development of the miRNA Profile

In this study, three left entities and three right entities of the eyes, lungs, and testes from normal mice were used for RNA-seq analysis. The genome-wide expression profiles of miRNAs were obtained from BGI Genomics (Beijing, China). The total RNAs were purified by gel cutting to separate the RNAs of the target fragment range, and library preparation was performed following BGI Genomics's standard procedure. Shortly, the adapters were ligated into the 3' end of RNA, and reverse transcriptase (RT) primers with unique molecular indices (UMIs) were added into the system, which were used for synthesizing the single-strand cDNA by reverse transcription. After cDNA amplification, target fragment separation, library quantification, and pooling cyclization, quantify control was performed on the constructed library, and then miRNA expression was quantified by counting the types of UMI tags. Finally, 1,431 miRNA signals were detected using the BGISEQ-500 sequencer, and DEMs were identified based on the p value (unpaired student's test, cutoff = 0.05) and fold change (FC) calculated by dividing the right expression value by the left one, where "NA" indicates that the expression value in the left organ is zero and is also considered to be differentially expressed. The expression profile data can be obtained from the GEO database (GEO: GSE146262).

### RNA Extraction

Total RNA was extracted using the RNAPure High-Purity Total RNA Rapid Extraction Kit (BioTeke, Beijing, China) according to the manufacturer's instructions. After DNase digestion, total RNA was eluted

**Table 1. Detailed Information for the Associations of miR-125a with Various Lung Diseases**

Lung Diseases	Evidence	PubMed Identifier (PMID)
Lung neoplasms	the results demonstrated that the panel of miRNA biomarkers (miR-125a-5p, miR-25, and miR-126) had the potential for the early detection of lung cancer;	25639977
Non-small-cell lung carcinoma	these preliminary data suggest that serum miR-125a-5p, miR-145, and miR-146a may be useful noninvasive biomarkers for the clinical diagnosis of non-small-cell lung cancer	25755772
Lung neoplasms	our results provide compelling evidence that miR-125a-5p, an epidermal growth factor-signaling-regulated miRNA, may function as a metastatic suppressor	19702827
Non-small-cell lung carcinoma	hsa-miR-125a-5p was poorly expressed in lung cancer cells, and it could enhance lung cancer cell invasion by upregulating hsa-miR-125a-5p	20719190
Lung neoplasms	miRNA hsa-miR-125a-3p activates p53 and induces apoptosis in lung cancer cells	24044511
Non-small-cell lung carcinoma	hsa-miR-125a-5p could upregulate Rock-1 and enhance invasion in lung cancer cells	20723344
Small-cell lung carcinoma	chemotherapy-regulated miRNA-125-HER2 pathway as a novel therapeutic target for trastuzumab-mediated cellular cytotoxicity in small-cell lung cancer	25833836
Non-small-cell lung carcinoma	miR-125a-3p targets MTA1 to suppress non-small-cell lung cancer cell proliferation, migration, and invasion	25998575
Lung carcinoma	miRNA-125a-5p plays a role as a tumor suppressor in lung carcinoma cells by directly targeting STAT3	28631574
Non-small-cell lung carcinoma	miR-125a-3p:Hsa-miR-125a-3p and hsa-miR-125a-5p are downregulated in non-small-cell lung cancer	20569443
Non-small-cell lung carcinoma	we showed that, compared to adjacent non-neoplastic lung tissues, the expressions of miR-125a-5p and let-7e were decreased in lung adenocarcinomas and squamous-cell lung carcinomas samples	22618509
Non-small-cell lung carcinoma	differential expression of miR-125a-5p and let-7e predicts the progression and prognosis of non-small-cell lung cancer	24945821
Lung carcinoma	miRNA expression profiles of granulocytic myeloid-derived suppressor cells from mice bearing Lewis lung carcinoma	27748875

with 30–80  $\mu$ L RNase-free water and stored at  $-80^{\circ}\text{C}$ . The purity and integrality of extracted total RNA were determined by the ratio of absorbance at 260 nm to that at 280 nm and via gel imaging.

#### Bulge-Loop Real-Time RT-PCR

For quantitative evaluation of miRNAs, bulge-loop real-time RT-PCR was performed. The detailed procedure has been described in a previous study.<sup>11</sup> In brief, the relative expression level of each miRNA was first normalized to small nuclear RNA U6 and then normalized to left group data values using  $2^{-\text{DDCt}}$  methodology. All the bulge-loop RT primers were purchased from RiboBio (Guangzhou, China), and the real-time PCR analysis was performed according to the manufacturer's instructions.<sup>11</sup>

#### Bioinformatic Analysis for miRNA Expression Profiles

Correlation analyses were performed between miRNA expression profiles in paired organs and those in mouse body fluids obtained from the GEO database (GEO: GSE111750 and GSE109655), homologous miRNA expression profiles in rat arterial plasma and venous plasma,<sup>33</sup> and homologous miRNA expression profiles in diverse human body fluids from small RNA-seq data across diverse biofluids<sup>34</sup> using the Spearman rank correlation test. The TAM v.2.0<sup>35</sup> tool was used to determine the enriched biological functions of the DEMs, and the MISIM<sup>36</sup> tool was used to calculate the miRNA functional similarity of the DEMs based on the miRNA-disease association dataset

in the HMDD database (v.3.0).<sup>37</sup> As both TAM and MISIM are designed for human miRNAs, here the mouse miRNAs were transformed into human orthologous miRNAs. The functional similarity networks were then constructed using Cytoscape software (v.3.6.1).<sup>38</sup> With regard to target analysis, we obtained the target genes of DEMs that have been experimentally verified from the miRTarBase database.<sup>39</sup> Following this, biological process and pathway enrichment analyses were conducted with the following ontology sources: GO Biological Processes;<sup>40</sup> Kyoto Encyclopedia of Genes and Genomes (KEGG) Pathway;<sup>41</sup> and Reactome Gene Sets using Metascape,<sup>42,43</sup> a web server for gene annotation and analysis. Furthermore, the terms were collected and grouped into clusters based on their membership similarities by the server, and the most statistically significant term within a cluster was chosen to represent the cluster.

#### Statistical Analysis

Data are presented as mean  $\pm$  SEM. Statistical significance of differences between groups was analyzed by Student's *t* test. Correlation analysis was performed by the Spearman rank correlation test. In all analyses,  $p < 0.05$  was considered to be significant.

#### SUPPLEMENTAL INFORMATION

Supplemental Information can be found online at <https://doi.org/10.1016/j.omtn.2020.07.006>.

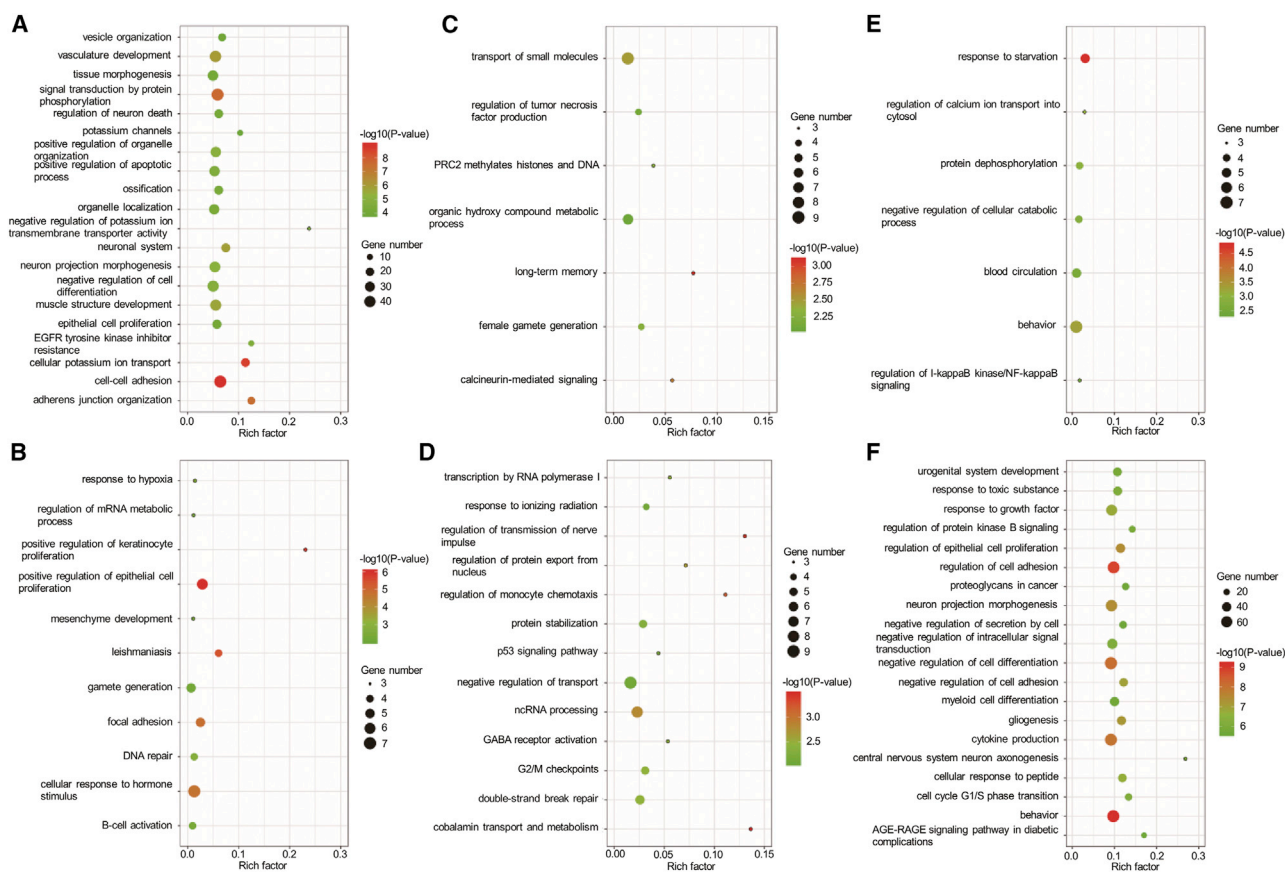


**Figure 6. Target Analysis for the DEMs**

(A–F) Biological process and pathway enrichment for target genes of the DEMs in the left (A) and right (B) eyes, left (C) and right (D) lungs, and left (E) and right (F) testes. The color of each point represents the value of  $-\log_{10}(p \text{ value})$ , and the different sizes of each point correspond to the number of genes represented in the term. The rich factor is the percentage of all the target genes found in the given ontology term.

## AUTHOR CONTRIBUTIONS

Q.C. and J.Y. conceived the study. Q.C. and J.Y. supervised the experiments. J.S., Y.Z., and C.C. performed bioinformatic analysis. C.H. conducted the biological experiments. All authors wrote the manuscript.

## CONFLICTS OF INTEREST

The authors declare no competing interests.

## ACKNOWLEDGMENTS

This work was supported by grants from the Natural Science Foundation of China (81670462, 81970440, and 81921001 to Q.C.), the Peking University Basic Research Program (BMU2020JC001), the Peking University Clinical Scientist Program (BMU2019LCKXJ001), and the Fundamental Research Funds for the Central Universities.

## REFERENCES

- Dyer, M.A., Rodriguez-Galindo, C., and Wilson, M.W. (2005). Use of preclinical models to improve treatment of retinoblastoma. *PLoS Med.* 2, e332.
- Cortes, J., Perez-García, J.M., Lombart-Cussac, A., Curigliano, G., El Saghir, N.S., Cardoso, F., Barrios, C.H., Wagle, S., Roman, J., Harbeck, N., et al. (2020). Enhancing global access to cancer medicines. *CA Cancer J. Clin.* 70, 105–124.
- Deng, S.Q., and Peng, H.J. (2020). Characteristics of and Public Health Responses to the Coronavirus Disease 2019 Outbreak in China. *J. Clin. Med.* 9, 575.
- Barr, R.D., Ries, L.A., Lewis, D.R., Harlan, L.C., Keegan, T.H., Pollock, B.H., and Bleyer, W.A.; US National Cancer Institute Science of Adolescent and Young Adult Oncology Epidemiology Working Group (2016). Incidence and incidence trends of the most frequent cancers in adolescent and young adult Americans, including “nonmalignant/noninvasive” tumors. *Cancer* 122, 1000–1008.
- Munuera-Gifre, E., Saez, M., Juvinyà-Canals, D., Rodríguez-Poncelas, A., Barrot-de-la-Puente, J.F., Franch-Nadal, J., Romero-Aroca, P., Barceló, M.A., and Coll-de-Tuero, G. (2020). Analysis of the location of retinal lesions in central retinographies of patients with Type 2 diabetes. *Acta Ophthalmol.* 98, e13–e21.
- Xu, Z., Shi, L., Wang, Y., Zhang, J., Huang, L., Zhang, C., Liu, S., Zhao, P., Liu, H., Zhu, L., et al. (2020). Pathological findings of COVID-19 associated with acute respiratory distress syndrome. *Lancet Respir. Med.* 8, 420–422.
- Vaganée, D., Daems, F., Aerts, W., Dewaide, R., van den Keybus, T., De Baets, K., De Wachter, S., and De Win, G. (2018). Testicular asymmetry in healthy adolescent boys. *BJU Int.* 122, 654–666.
- Bao, X.Y., and Cao, J. (2019). MiRNA-138-5p protects the early diabetic retinopathy by regulating NOVA1. *Eur. Rev. Med. Pharmacol. Sci.* 23, 7749–7756.

9. Zheng, J., Zhang, Y., Cai, S., Dong, L., Hu, X., Chen, M.B., and Zhu, Y.H. (2020). MicroRNA-4651 targets bromodomain-containing protein 4 to inhibit non-small cell lung cancer cell progression. *Cancer Lett.* *476*, 129–139.
10. van Agthoven, T., Eijkenboom, W.M.H., and Looijenga, L.H.J. (2017). microRNA-371a-3p as informative biomarker for the follow-up of testicular germ cell cancer patients. *Cell Oncol. (Dordr.)* *40*, 379–388.
11. Gao, Y., Yang, W., Jin, L., Xue, L., Yang, J., and Cui, Q. (2020). Profiling and bioinformatic analysis reveal differential microRNA expression in the left and right kidneys in normal mice. *FEBS Lett.* *594*, 636–645.
12. Zhang, Q., Lu, M., and Cui, Q. (2008). SNP analysis reveals an evolutionary acceleration of the human-specific microRNAs. *Nat. Prec.* Published online July 29, 2008. <https://doi.org/10.1038/npre.2008.2127.1>.
13. Kozomara, A., and Griffiths-Jones, S. (2014). miRBase: annotating high confidence microRNAs using deep sequencing data. *Nucleic Acids Res.* *42*, D68–D73.
14. Wang, J., Chen, J., and Sen, S. (2016). MicroRNA as Biomarkers and Diagnostics. *J. Cell. Physiol.* *231*, 25–30.
15. Chen, G., Wang, J., and Cui, Q. (2013). Could circulating miRNAs contribute to cancer therapy? *Trends Mol. Med.* *19*, 71–73.
16. Shi, L., Kim, A.J., Chang, R.C., Chang, J.Y., Ying, W., Ko, M.L., Zhou, B., and Ko, G.Y. (2016). Deletion of miR-150 Exacerbates Retinal Vascular Overgrowth in High-Fat-Diet Induced Diabetic Mice. *PLoS ONE* *11*, e0157543.
17. Zhang, Q.-L., Wang, W., Alatan TUYA, Dongmei, Lu, Z.-J., Li, L.-L., and Zhang, T.-Z. (2018). Down-regulated miR-187 promotes oxidative stress-induced retinal cell apoptosis through P2X7 receptor. *Int. J. Biol. Macromol.* *120* (Pt. A), 801–810.
18. Abhari, A., Zarghami, N., Shahnavi, V., Barzegar, A., Farzadi, L., Karami, H., Zununi Vahed, S., and Nouri, M. (2014). Significance of microRNA targeted estrogen receptor in male fertility. *Iran. J. Basic Med. Sci.* *17*, 81–86.
19. Grinchuk, O.V., Jenjaroenpun, P., Orlov, Y.L., Zhou, J., and Kuznetsov, V.A. (2010). Integrative analysis of the human cis-antisense gene pairs, miRNAs and their transcription regulation patterns. *Nucleic Acids Res.* *38*, 534–547.
20. Dabaja, A.A., Mielnik, A., Robinson, B.D., Wosnitzer, M.S., Schlegel, P.N., and Paduch, D.A. (2015). Possible germ cell-Sertoli cell interactions are critical for establishing appropriate expression levels for the Sertoli cell-specific MicroRNA, miR-202-5p, in human testis. *Basic Clin. Androl.* *25*, 2.
21. Das, M.K., Evensen, H.S.F., Furu, K., and Haugen, T.B. (2019). miRNA-302s may act as oncogenes in human testicular germ cell tumours. *Sci. Rep.* *9*, 9189.
22. Hughes, J.L., Lackie, P.M., Wilson, S.J., Church, M.K., and McGill, J.I. (2006). Reduced structural proteins in the conjunctival epithelium in allergic eye disease. *Allergy* *61*, 1268–1274.
23. Tang, S., Le-Ruppert, K.C., and Gabel, V.P. (1994). Expression of intercellular adhesion molecule-1 (ICAM-1) and vascular cell adhesion molecule-1 (VCAM-1) on proliferating vascular endothelial cells in diabetic epiretinal membranes. *Br. J. Ophthalmol.* *78*, 370–376.
24. Deng, L., and Gwiazda, J.E. (2012). Anisometropia in children from infancy to 15 years. *Invest. Ophthalmol. Vis. Sci.* *53*, 3782–3787.
25. Zhong, X., Ge, J., Nie, H., and Smith, E.L., 3rd (2004). Compensation for experimentally induced hyperopic anisometropia in adolescent monkeys. *Invest. Ophthalmol. Vis. Sci.* *45*, 3373–3379.
26. Siegwart, J.T., Jr., and Norton, T.T. (2010). Binocular lens treatment in tree shrews: Effect of age and comparison of plus lens wear with recovery from minus lens-induced myopia. *Exp. Eye Res.* *91*, 660–669.
27. Zaka-Ur-Rab, S. (2006). Evaluation of relationship of ocular parameters and depth of anisotropic amblyopia with the degree of anisometropia. *Indian J. Ophthalmol.* *54*, 99–103.
28. Greenough, A., Ahmed, T., and Broughton, S. (2006). Unilateral pulmonary agenesis. *J. Perinat. Med.* *34*, 80–81.
29. Oster, J. (1971). Varicocele in children and adolescents. An investigation of the incidence among Danish school children. *Scand. J. Urol. Nephrol.* *5*, 27–32.
30. Akbay, E., Cayan, S., Doruk, E., Duce, M.N., and Bozlu, M. (2000). The prevalence of varicocele and varicocele-related testicular atrophy in Turkish children and adolescents. *BJU Int.* *86*, 490–493.
31. Kim, D., Sung, Y.M., Park, J., Kim, S., Kim, J., Park, J., Ha, H., Bae, J.Y., Kim, S., and Baek, D. (2016). General rules for functional microRNA targeting. *Nat. Genet.* *48*, 1517–1526.
32. Dragomir, M.P., Knutsen, E., and Calin, G.A. (2018). SnapShot: Unconventional miRNA Functions. *Cell* *174*, 1038–1038.e1.
33. Xu, W., Zhou, Y., Xu, G., Geng, B., and Cui, Q. (2017). Transcriptome analysis reveals non-identical microRNA profiles between arterial and venous plasma. *Oncotarget* *8*, 28471–28480.
34. Srinivasan, S., Yeri, A., Cheah, P.S., Chung, A., Danielson, K., De Hoff, P., Filant, J., Laurent, C.D., Laurent, L.D., Magee, R., et al. (2019). Small RNA Sequencing across Diverse Biofluids Identifies Optimal Methods for exRNA Isolation. *Cell* *177*, 446–462.e16.
35. Li, J., Han, X., Wan, Y., Zhang, S., Zhao, Y., Fan, R., Cui, Q., and Zhou, Y. (2018). TAM 2.0: tool for MicroRNA set analysis. *Nucleic Acids Res.* *46* (W1), W180–W185.
36. Li, J., Zhang, S., Wan, Y., Zhao, Y., Shi, J., Zhou, Y., and Cui, Q. (2019). MISIM v2.0: a web server for inferring microRNA functional similarity based on microRNA-disease associations. *Nucleic Acids Res.* *47* (W1), W536–W541.
37. Huang, Z., Shi, J., Gao, Y., Cui, C., Zhang, S., Li, J., Zhou, Y., and Cui, Q. (2019). HMDD v3.0: a database for experimentally supported human microRNA-disease associations. *Nucleic Acids Res.* *47* (D1), D1013–D1017.
38. Shannon, P., Markiel, A., Ozier, O., Baliga, N.S., Wang, J.T., Ramage, D., Amin, N., Schwikowski, B., and Ideker, T. (2003). Cytoscape: a software environment for integrated models of biomolecular interaction networks. *Genome Res.* *13*, 2498–2504.
39. Chou, C.H., Shrestha, S., Yang, C.D., Chang, N.W., Lin, Y.L., Liao, K.W., Huang, W.C., Sun, T.H., Tu, S.J., Lee, W.H., et al. (2018). miRTarBase update 2018: a resource for experimentally validated microRNA-target interactions. *Nucleic Acids Res.* *46* (D1), D296–D302.
40. Ashburner, M., Ball, C.A., Blake, J.A., Botstein, D., Butler, H., Cherry, J.M., Davis, A.P., Dolinski, K., Dwight, S.S., Eppig, J.T., et al. (2000). The Gene Ontology Consortium (2000). Gene ontology: tool for the unification of biology. *Nat. Genet.* *25*, 25–29.
41. Kanehisa, M., Furumichi, M., Tanabe, M., Sato, Y., and Morishima, K. (2017). KEGG: new perspectives on genomes, pathways, diseases and drugs. *Nucleic Acids Res.* *45* (D1), D353–D361.
42. Zhou, Y., Zhou, B., Pache, L., Chang, M., Khodabakhshi, A.H., Tanaseichuk, O., Benner, C., and Chanda, S.K. (2019). Metascape provides a biologist-oriented resource for the analysis of systems-level datasets. *Nat. Commun.* *10*, 1523.
43. Jassal, B., Matthews, L., Viteri, G., Gong, C., Lorente, P., Fabregat, A., Sidiropoulos, K., Cook, J., Gillespie, M., Haw, R., et al. (2020). The reactome pathway knowledgebase. *Nucleic Acids Res.* *48* (D1), D498–D503.